European Journal of Pharmaceutical Sciences 69 (2015) 26–36

Contents lists available at ScienceDirect

European Journal of Pharmaceutical Sciences

journal homepage: www.elsevier.com/locate/ejps

Real-time UV imaging identifies the role of pH in insulin dissolution behavior in hydrogel-based subcutaneous tissue surrogate

Sabrine S. Jensen, Henrik Jensen, Claus Cornett, Eva H. Møller [1], Jesper Østergaard *

Department of Pharmacy, Faculty of Health and Medical Sciences, University of Copenhagen, Universitetsparken 2, DK-2100 Copenhagen, Denmark

ARTICLE INFO

Article history:
Received 13 November 2014
Received in revised form 17 December 2014
Accepted 17 December 2014
Available online 7 January 2015

Keywords:
Dissolution
Hydrogel
Insulin
Mass transport
Microenvironmental pH
UV imaging

ABSTRACT

For parenteral biopharmaceuticals, subcutaneous diffusion and, in the case of solid implants or suspensions, dissolution may govern the clinical profile of the drug product. Insight into the dissolution and diffusion processes of biopharmaceuticals after parenteral administration is fundamental in the development of new protein drug formulations. Using insulin as a model compound, the aim of this work was to develop a UV imaging-based method to study the real-time dissolution and diffusion behavior of solid protein drugs under stagnant conditions in a hydrogel matrix mimicking the subcutaneous tissue. Dissolution of proteins and peptides is a complex phenomenon as it may be coupled to the complicated acid base properties of these substances. UV imaging allowed the real-time dissolution and diffusion processes of insulin at different pH values and of different insulins to be studied. Dissolution rates were obtained, and the quantitative performance of the developed UV imaging method was verified. It was shown that the UV imaging dissolution method was able to differentiate between the behavior of different insulins and that human insulin dissolution was highly dependent on pH. pH effects in the microenvironment of the human insulin compacts at pH 7.40 and 3.00 were observed by UV–Vis imaging, explaining the different dissolution kinetics of human insulin at pH 7.40 and 3.00 as compared to pH 5.40. In conclusion, UV–Vis imaging may be a useful tool for studying dissolution, diffusion and pH effects in the vicinity of solid protein drug in a hydrogel matrix with the aim of achieving a better understanding of *in vivo* dissolution processes.

1. Introduction

Peptide and protein therapeutics constitute an increasing fraction of the drug products available for treatment of patients. Most peptide and protein therapeutics are administrated parenterally due to their low permeability across biological membranes and chemical and enzymatic instability in the gastrointestinal tract (Lin, 2009; McDonald et al., 2010). The implications of the administration pathway – that patients must be injected, often daily – render peptide and protein drug products with prolonged effect, minimizing the number of injections for patient, highly desirable. Examples of parenterals with prolonged release are solid implants and suspensions. In the development of solid drug formulations, dissolution testing of the active pharmaceutical ingredient is required as a characterization tool as well as in quality control. Despite a demand for *in vitro* dissolution models capable of characterizing the dissolution and release from sustained release parenteral drug formulations, at present, standard compendial *in vitro* dissolution models do not exist for these formulations (Burgess et al., 2002; Martinez et al., 2008). In compendial *in vitro* dissolution models, the dissolution methods rely on bulk solution concentration measurements as a function of time due to the applied stirring or flow. Using these methods it is thus not possible to study dissolution and release into a "solid" material such as a hydrogel. This may result in loss of important information when detailed insights into the dissolution process are required. Furthermore, *in vivo*, parenterally administrated peptide and protein formulations are not subjected to convective mass transport to the same extent as the available compendial *in vitro* dissolution models may provide. A suitable *in vitro* model simulating the *in vivo* conditions, e.g. with respect to mass transport and matrix morphology may provide valuable insight into the dissolution, release and diffusion processes of peptide and protein drugs intended for parenteral administration. Such information would be useful in the development of new peptide and protein formulations. Our hypothesis is that an *in vitro* dissolution method able to character-

* Corresponding author. Tel.: +45 3533 6138; fax: +45 3533 6001.
E-mail addresses: sabrine.smedegaard@sund.ku.dk (S.S. Jensen), henrik.jensen@sund.ku.dk (H. Jensen), claus.cornett@sund.ku.dk (C. Cornett), ehom@novonordisk.com (E.H. Møller), jesper.ostergaard@sund.ku.dk (J. Østergaard).
[1] Present address: Novo Nordisk A/S, Novo Nordisk Park, DK-2760 Måløv, Denmark.

http://dx.doi.org/10.1016/j.ejps.2014.12.015
0928-0987/

ize the real-time dissolution and diffusion processes in the vicinity of the drug compound in a matrix mimicking the subcutaneous tissue, e.g. a hydrogel, may provide a better understanding of the *in vivo* dissolution and diffusion of peptide and protein formulations intended for subcutaneous administration.

A closer look into dissolution and release processes may be obtained by different imaging techniques including, magnetic resonance imaging (MRI) (Fyfe and Blazek-Welsh, 2000; Nott, 2010; Richardson et al., 2005), Fourier transform infrared (FTIR) imaging (Kazarian and van der Weerd, 2008; Kazarian and Ewing, 2013; Kimber et al., 2011), fluorescence imaging (Adler et al., 1999; Bajwa et al., 2006; Brandl et al., 2010), and UV imaging (Boetker et al., 2011; Østergaard et al., 2011). UV imaging provides the ability to generate temporally and spatially resolved data in the form of images from the absorbance of UV light (Østergaard et al., 2010). UV imaging enables real-time drug dissolution, release and transport studies in transparent media without the need of labeling the drug compound. UV imaging has mainly been used for studying the dissolution behavior of active pharmaceutical ingredients in a flow through setup (Boetker et al., 2011; Hulse et al., 2012; Niederquell and Kuentz, 2014; Nielsen et al., 2013; Østergaard et al., 2014a; Qiao et al., 2013).

Hydrogels are widely employed as delivery vehicles. However, hydrogels have also been suggested as models for soft tissues (Allababidi and Shah, 1998; Gietz et al., 1998; Klose et al., 2009; Lee et al., 2009; Liang et al., 2006; Ye et al., 2012a,b) to facilitate a better understanding of the release and mass transport processes upon *in vivo* administration of parenteral formulations.

Recently, hydrogel matrixes were found to be compatible with the UV imaging setup. Drug diffusion (Ye et al., 2011), drug release (Ye et al., 2012a, 2011), release and partitioning from lipophilic solutions (Ye et al., 2012b), and release from particulate dosage forms (Sarnes et al., 2013) in hydrogels mimicking the subcutaneous tissue have been studied by UV imaging. From these studies it was shown that important information in relation to drug release in terms of drug distribution and diffusion coefficients may be obtained using UV imaging. Recently, we showed that UV imaging also allows human insulin diffusion in hydrogels to be studied in real-time, and that the human insulin self-association properties were reflected in the diffusion behavior in the agarose gel matrixes mimicking the subcutaneous tissue (Jensen et al., 2014). The overall aim of our current research is to develop and establish *in vitro* release models capable of characterizing and visualizing the release of peptide and protein formulations intended for subcutaneous administration in a matrix mimicking the subcutaneous tissue. The objective of the present study was to develop a UV imaging-based method to study the real-time dissolution behavior of protein drugs in the immediate vicinity of the solid compound under stagnant conditions in a hydrogel matrix mimicking the subcutaneous tissue. Moreover, the objective was to characterize drug transport in the surrounding hydrogel matrix including the assessment of potential local pH effects on dissolution. Using insulin as a model compound, the dissolution behavior of human insulin at pH 3.00, 5.40, and 7.40 and bovine insulin and protamine insulin at pH 7.40 were investigated by UV imaging.

2. Materials and methods

2.1. Chemicals

Agarose (type I), lyophilized bovine insulin, and protamine sulfate were obtained from Sigma–Aldrich (St. Louis, MO, USA). Amorphous recombinant human insulin (rDNA) was obtained from Millipore (Bedford, MA, USA). Methyl orange was obtained from J.D. Riedel-E.de Haen A.G. (Berlin, Germany). Bromothymol blue, citric acid anhydrate, hydrochloric acid, methyl red, sodium acetate, sodium dihydrogenphosphate monohydrate and sodium hydroxide were obtained from Merck (Darmstadt, Germany).

Dissolution experiments were performed in buffered solutions with an ionic strength of 0.15 M. Phosphate buffered solutions with a concentration of 0.067 M and 0.17 M at pH 7.40 and 3.00, respectively, were prepared by dissolving an appropriate amount of sodium dihydrogenphosphate monohydrate in deionized water followed by pH adjustment to 7.40 and 3.00 using 5 M NaOH and 6.85 M HCl, respectively. A 0.17 M acetate buffer solution pH 5.40 was prepared by dissolving an appropriate amount of sodium acetate trihydrate in deionized water and adjusting the pH to 5.40 using 5 M NaOH.

Stock solution of methyl orange (3.06×10^{-4} M) was prepared according to Ph.Eur (Council of Europe, 2014). Stock solutions of methyl red (7.42×10^{-4} M) and bromothymol blue (9.61×10^{-4} M) were prepared by dissolving a weighed amount of the pH indicator in 60% (v/v) ethanol (96%) and 0.1 M sodium hydroxide, respectively, and adding demineralized water to volume. Hydrochloric acid, sodium hydroxide, acetate buffered and phosphate buffered solutions were prepared for constructing absorbance – pH profiles of the pH indicators.

2.2. Preparation of protamine insulin

In the present study amorphous protamine insulin was prepared by adding an aliquot of 0.74 ml phosphate buffered, pH 7.40, 5.00 mg/ml protamine sulfate solution to 20.00 ml phosphate buffered, pH 7.40, 1.78 mg/ml insulin solution (phenol or cresol was not added to the insulin solution). Precipitation of protamine insulin was observed immediately upon addition of protamine sulfate to the insulin solution. The precipitate of protamine insulin was left at room temperature for 96 h. The precipitate was isolated and collected by filtering the suspension through a cellulose filter (HAWP) with a pore size of 0.45 μm (MF Millipore Membrane Filters) while suction was applied. The precipitate was placed in a desiccator with silica at ambient temperature (22.0 ± 0.5 °C) for 24 h to dry.

2.3. Preparation of agarose hydrogels

Agarose powder corresponding to 1.5, 0.5, and 0.5% (w/v) was suspended in buffered solution at pH 3.00, 5.40 and 7.40, respectively. The suspensions were heated to 98 °C for 20 min to dissolve the agarose, and the agarose solutions were transferred to a quartz cell (7.5 mm × 3.0 mm × 63 mm (H × W × L)) equipped with a sample holder. The cells were left at ambient temperature for at least 1.5, 1.0 and 1.0 h for gelation of the agarose gels at pH 3.00, 5.40 and 7.40, respectively. In studying the microenvironmental pH during insulin dissolution a volume of the pH indicator stock solution was added to the agarose solution just before it was transferred to the quartz cell. The pH within the hydrogel matrix was not affected by the added pH indicator, because the concentration of the pH indicator (7.5×10^{-5} M methyl orange, 5.2×10^{-5} M methyl red and 6.7×10^{-5} M bromothymol blue at pH 3.00, 5.40 and 7.40, respectively) was much lower than the buffer concentration (0.17, 0.17 and 0.067 M at pH 3.00, 5.40 and 7.40, respectively).

2.4. Preparation of compacts

Compacts for the UV imaging dissolution studies were prepared by transferring samples of solid amorphous human insulin, bovine insulin, protamine insulin, and protamine (5–7 mg) into a stainless steel cylinder (2 mm inner diameter (id)) placed in a manual press (Actipress, Paraytec Ltd., York, UK). In case of compacts with two

components, the components were mixed in a mortar before a weighed amount of the physical mixture was transferred to the cylinder in the manual press. A Quickset MINOR torque screwdriver (Torqueleader, M. H. H. Engineering Co. Ltd., England) was used to compress the samples at a constant torque of 0.60 N m.

Inspections of the compact surfaces and microenvironmental pH changes were performed under a Digital Blue QX-5 microscope with a magnification rage of 10–200 (Prime Entertainment Company, China) or a Dino-Lite Digital microscope with a magnification range of 20–200 (AnMo Electronics Corporation, Hsinchu, Taiwan).

2.5. UV–Vis imaging

UV–Vis imaging measurements were performed using an Actipix SDI300 dissolution imaging system (Paraytec Ltd, York, UK) equipped with a CADISS-2 cartridge. A quartz cell with the dimensions 7.5 mm × 3.0 mm × 63.0 mm (H × W × L) was placed in the cartridge. The detection area of the UV–Vis imaging system was 7.0 mm × 9.0 mm consisting of 1000 × 1280 pixels (the pixels were binned 4 × 4). Due to the sample holder in the quartz cell, the effective imaging area was 4.5 × 9.0 mm. A pulsed Xenon lamp was used as the light source, and imaging was performed at 214, 232, or 280 nm in the UV wavelength range and at 510 or 610 nm in the visible wavelength range. Images were recorded and analyzed using the Actipix software version 1.4 (Paraytec Ltd., York, UK). Images were recorded with a rate of 15 images per min, and the integration time was 10 ms. The measured intensities were converted into absorbance by the Actipix software. By applying a calibration curve the apparent concentration within the effective imaging area was determined as a function of time.

UV imaging was performed by acquiring dark images with the lamp turned off (10 s) followed by reference images (10 s) with the quartz cell filled with the dissolution medium, phosphate buffered solution or agarose hydrogel. During this initial period a solid stainless steel cylinder was placed in the sample holder. The imaging was paused after 60 s of data collection, and the stainless steel cylinder was replaced by a compact of the sample. The data collection was hereafter resumed. The experiments were carried out at ambient temperature (23.5 ± 1.5 °C), and the experiments were performed in triplicate.

2.6. UV imaging data analysis

2.6.1. Determination of the dissolution rate

For each sample the amount of dissolved insulin as a function of time was determined from the UV absorbance maps obtained using an area of 4.48 ± 0.05 mm × 9.00 mm, which corresponds to a volume of the dissolution medium of 120 µl (4.48 × 3.00 × 9.00 mm^3). The dissolution rates were determined from the linear region of the dissolution profiles during the first 30–180 min of the dissolution process (as long as the sample remained within the imaging area). Due to different dissolution rates, solubilities and diffusion coefficients of the insulins under the applied conditions, the time depended on the specific insulin sample subject to investigation.

2.6.2. Modeling of the dissolution profiles

In order to characterize drug transport in the hydrogel matrixes, the dissolution profiles were modeled by applying a derivation of Fick's second law. To simplify the model, it was assumed that the sample compact was a plane source deposited initially at a plane surface (at a distance: $x = 0$), and that the initial concentration is zero throughout the semi-infinite medium (at a distance: $x > 0$). Assuming a constant surface concentration (C_0), the following derivation of Fick's second law was applied (Crank, 1975):

$$M_t = 2 \cdot A \cdot C_0 \cdot \sqrt{\left(\frac{D \cdot t}{\pi}\right)} \quad (1)$$

where M_t is the amount of diffusing substance which has entered the dissolution matrix in time t, when the initial concentration in the medium is zero; A is the surface area of the compact in contact with the dissolution medium, and D is the diffusion coefficient. Eq. (1) is applicable for one-dimensional diffusion, and it is assumed that there is no resistance to transport at the interface. Furthermore, the diffusion coefficient is assumed to be constant.

2.7. Quantification by HPLC analysis

The amount of dissolved insulin in selected agarose matrixes were quantified by HPLC analysis to substantiate the results obtained by UV imaging. The hydrogel matrix containing the dissolved insulin was isolated, weighed, and cut in small pieces where after 1.0 ml phosphate buffered solution was added. After 24 h the resulting sample was filtered through a cellulose filter (0.2 µm pore size) (Agilent Technologies, Waldbronn, Germany) and the filtrate was analyzed by HPLC. The HPLC system consisted of a Merck Hitachi pump L-7100, column oven L-7350, autosampler L-7200, interface D-7000 and UV detector L-7400 (Merck Hitachi, Schaumburg, IL, USA). The samples were analyzed by reverse phase chromatography on a Symmetry Shield RP C18 intelligent speed column with dimensions of 3.9 mm (id) × 20.0 mm, a particle size of 3.5 µm and a pore size of 100 Å (Waters Corporation, Milford, MA, USA). A Phenomenex Gemini C18 security guard (4 × 3.0 mm id) (Phenomenex, Torrance, CA, USA) was placed in front of the column. The column oven was set at 30 °C. The injection volume was 15 µl, the analysis was performed at a flow rate of 1 ml/min, and the UV absorbance was detected at a wavelength of 215 nm. Data were collected using Merck Hitachi HPLC system manager software version 4.0 (Merck Hitachi, Schaumburg, IL, USA). Using eluent A comprising 0.2 M sodium sulfate, 0.04 M sodium phosphate at pH 3.6, and 10% (v/v) acetonitrile, and eluent B consisting of 70% (v/v) acetonitrile and 30% (v/v) MQ water, the HPLC analysis was performed by a linear gradient method: 0 min 80% (v/v) A, 1.4 min 80% (v/v) A, 4.0 min 55% (v/v) A, 4.1 min 80% (v/v) A, and 8.0 min 80% (v/v) A.

2.8. X-ray Powder Diffraction measurements

X-ray Powder Diffraction (XRPD) measurements of the human insulin, bovine insulin and protamine insulin and the prepared insulin compacts before and after the dissolution experiments were performed. XRPD was performed using a PANalytical X'Pert Pro θ/θ diffractometer equipped with a PIXcel detector (PANalytical B.V., Almelo, The Netherlands). Cu radiation with a wavelength of 1.54 Å was used to perform a continuous scan in an angle from 2° to 35°. A current of 40 mA was applied. Data were collected using X'Pert data collector version 2.2 and analyzed with X'Pert highscore plus version 2.2d (PANalytical B.V., Almelo, The Netherlands).

2.9. Apparent solubility

The apparent solubilities of human insulin, bovine insulin, protamine insulin and protamine in buffered solutions at pH 3.00, 5.40 and/or 7.40 were determined at ambient temperature (23.0 ± 1.5 °C). Samples were prepared by adding a weighed amount of insulin or protamine to 1.50–2.00 ml of buffered solution. After 2, 3, 4 and/or 22, 23, and 24 h samples were withdrawn and filtrated through a cellulose filter (0.2 µm pore size; Agilent Technologies, Waldbronn, Germany). The filtrate was diluted with

buffered solution, and the absorbance was measured in a closed ended quartz cells type 20/O C (Starna Scientific Ltd., Hainault, Essex, UK) with a light path of 1 mm at a wavelength of 214 or 280 nm by UV imaging. The concentrations of human insulin at pH 3.00 and protamine at pH 7.40 were only measured in the samples after 2, 3, and 4 h, due to complete dissolution of insulin under the applied conditions. An average of the concentrations measured in the samples after 22, 23, and 24 h was taken as a measure of the apparent solubility of human insulin at pH 5.40 and 7.40 as well as for bovine insulin and protamine insulin at pH 7.40.

2.10. UV–Vis absorbance spectra

UV–Vis absorbance spectra were performed on UV-1700 spectrophotometer (Shimadzu, Suzhou Instruments manufacturing Ltd., Suzhou, China) in a wavelength range from 200–400 nm or 400–750 nm. Quarts cells with a 10.00 mm light path were used for the measurements.

2.11. Thermogravimetric analysis

Thermogravimetric analysis (TGA) of human insulin, bovine insulin and protamine insulin were performed on a Discovery TGA (TA Instruments, New Castle, DE, USA). Solid samples in platinum HT pans were heated by a ramp from 25 to 400 °C at 10 °C/min to determine the water content and the temperature of decomposition. The measurements were performed in an inert atmosphere of N_2.

3. Results and discussion

The dissolution of insulin was studied under stagnant conditions in an agarose gel matrix in order to mimic the subcutaneous tissue environment. Under the conditions realized in the *in vitro* model, the mass transport in the dissolution media is governed by diffusion, which is one of the most important transport phenomena in subcutaneous tissue (Levick, 1987; Richter et al., 2012; Swabb et al., 1974; Swartz and Fleury, 2007). The *in vitro* dissolution method is different from conventional dissolution and release testing models in which convection is the main contributing factor to mass transport. Previously, SEM pictures of agarose hydrogel matrixes have shown that the hydrogel matrixes have a porous structure and the pore size decreased with increasing agarose concentration (Jensen et al., 2014). In several studies, the pore size of agarose hydrogels has been determined, and the pore size generally ranges from 100–900 nm at agarose concentrations between 2.0–0.5% (w/v) (Maaloum et al., 1998; Pluen et al., 1999; Tinland et al., 1996; Xiong et al., 2005). Despite a relative large variability of the measured pore sizes obtained in the different studies, the agarose hydrogel pore size is large relative to the size of the insulin monomer, dimer, and hexamer having hydrodynamic radii in the range 1.5–3.0 nm (Jensen et al., 2014; Kadima et al., 1993). Previous studies indicate that insulin, irrespective of the self-association state of insulin, is able to diffuse freely in 1.5 and 0.5% (w/v) agarose hydrogels at pH 3.00 and 7.40, respectively (Jensen et al., 2014).

3.1. The effect of pH on the dissolution behavior of human insulin

The dissolution process of amorphous human insulin in stagnant phosphate buffer at pH 7.40 was monitored in real-time using UV imaging (Fig. 1). From the obtained UV absorbance maps it can be seen that the dissolution cell, with time, appears to be filled from the bottom and up. UV imaging is capable of visualizing different mass transport phenomena and the above mentioned observations are most likely due to the formation of a density gradient as observed previously for other systems (Gaunø et al., 2013; Østergaard et al., 2011). The density gradient made these experiments unsuitable for quantification of the dissolution rate, because the dissolved drug compound escaped the UV imaging area after e.g. approximately 15 min for human insulin at pH 7.40. An agarose hydrogel was therefore introduced as a dissolution medium to suppress the effect of the density gradients on the dissolution patterns (Garcia-Ruiz et al., 2001; Gaunø et al., 2013; Lorber et al., 2009). Dissolution of human insulin compacts in agarose hydrogel matrixes at pH 7.40 showed the formation of a symmetrical UV absorbance map around the surface of the compact (Fig. 2A). This indicates that the mass transport is mainly diffusive, and that the natural convection, due to the density differences in the system, has been efficiently suppressed. Also, the amount of drug release could be monitored for longer time intervals.

The physiological pH of the subcutaneous tissue is close to pH 7.4 (Kinnunen and Mrsny, 2014), and consequently a pH of 7.40 is most relevant in *in vitro* dissolution and release testing of drug compounds for subcutaneous administration. In the development of the current *in vitro* dissolution model, experiments were also performed at pH 3.00 and 5.40, because the physicochemical properties of the selected model drug, insulin, are known to be pH dependent. Experiments at pH 3.00, 5.40, and 7.40 were thus performed to gain knowledge in the dissolution behavior of insulin under different conditions as well as to obtain a better understanding of the developed *in vitro* method. The spatially and temporally resolved UV absorbance maps (Fig. 2) were converted into dissolution profiles showing the dissolved mass of insulin as a function of time (Fig. 3). Calibration curves for converting UV absorbance into concentration are shown in supplementary data (Fig. A.1). Dissolution profiles of amorphous human insulin in agarose hydrogel matrixes at different pH values showed that the dissolution of human insulin decreased in the following order pH 3.00 > 7.40 > 5.40 as expected. The dissolution rate of human insulin in the agarose hydrogel matrix at pH 3.00, 5.40, and 7.40, respectively, was determined from the slope of the dissolution profiles (Fig. 3), and the surface area of the compact in contact with the dissolution medium (Table 1). Different agarose concentrations were used to prepare the hydrogels at the different pH values due to a decreased gelling ability of agarose hydrogels at acidic conditions. At pH 5.40 and 7.40 an agarose concentration of 0.5% (w/v) was used, while the agarose concentration was increased to 1.5% (w/v) at pH 3.00. Recently, it was shown that the apparent diffusivity of insulin was not affected by increasing the agarose concentration from 0.5% to 1.5% (w/v) in similar hydrogel matrixes at pH 3.00 (Jensen et al., 2014). The different agarose concentrations are therefore not expected to have an effect on the dissolution behavior of human insulin.

The quantitative performance of the UV imaging setup was investigated by comparing the results obtained by UV imaging with results obtained by extracting the dissolved human insulin from the hydrogel and quantifying this amount by HPLC. The amount of dissolved human insulin (mass ± SD) at pH 7.40 was determined to 81.0 ± 1.5 and 74.5 ± 5.3 μg after 60 min by UV imaging and HPLC, respectively ($n = 3$). Thus, good agreement between the results was observed, and the applied UV imaging method was found applicable for determining dissolution rates. The larger SDs of the results obtained by HPLC may be due to the sample preparation prior to the HPLC analysis.

XRPD measurements of the human insulin powder and the compacts of human insulin before and after the dissolution experiments showed that insulin remained amorphous throughout the experiments at pH 3.00, 5.40, and 7.40. Hence, XRPD measurements established that the lower dissolution rate of human insulin at pH 5.40 and 7.40 as compared to pH 3.00 was not due to solid

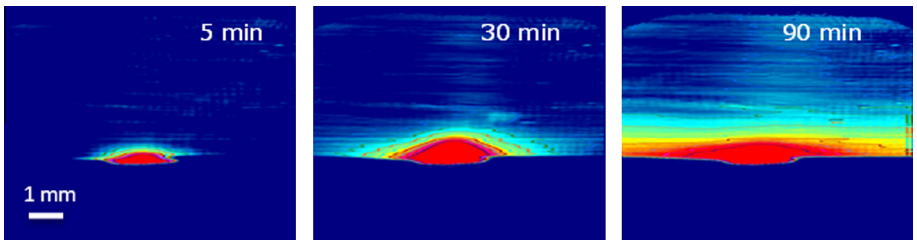

Fig. 1. UV absorbance maps of the dissolution of amorphous human insulin in stagnant 67 mM phosphate buffer, pH 7.40, measured at 280 nm. Intense red color indicates high absorbance and the contours represent the iso-absorbance lines. The contour offset is 100 mAU and the contour interval is 100 mAU. The measurements were performed at 23.0 ± 1.5 °C. (For interpretation of the references to color in this figure legend, the reader is referred to the web version of this article.)

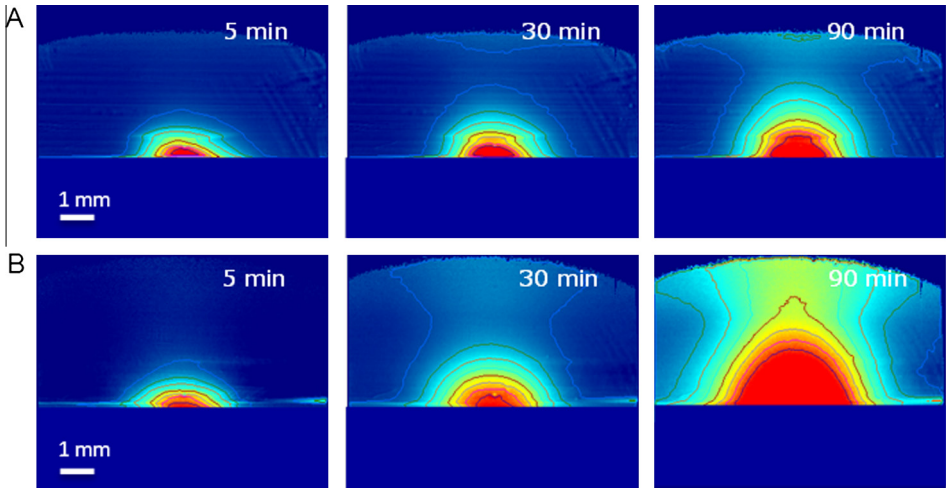

Fig. 2. UV absorbance maps of the dissolution of amorphous human insulin in (A) 0.5% (w/v) agarose hydrogel, pH 7.40, and (B) 1.5% (w/v) agarose gel, pH 3.00, measured at 280 nm. Intense red color indicates high absorbance and the contours represent the iso-absorbance lines. The contour offset is 100 mAU (light blue) and the contour interval is 100 mAU. The measurements were performed at 23.0 ± 1.5 °C. (For interpretation of the references to color in this figure legend, the reader is referred to the web version of this article.)

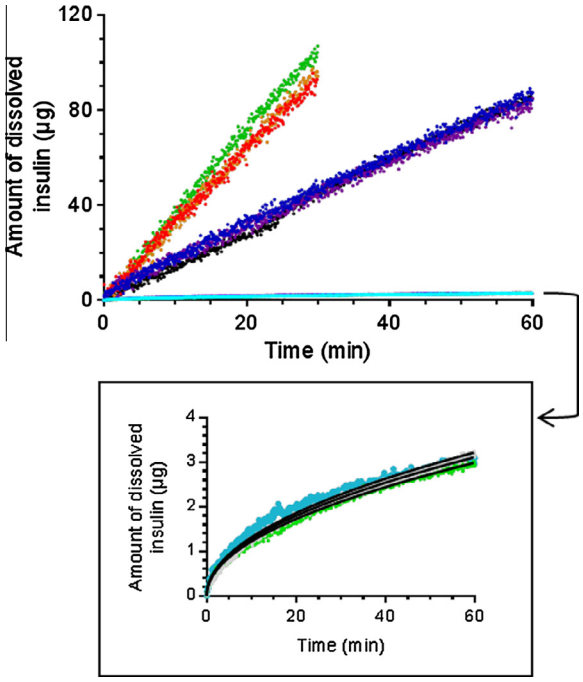

Fig. 3. Dissolution profiles for human insulin in 1.5% (w/v) agarose gel, pH 3.00, (●, ●, ●), 0.5% (w/v) agarose gel, pH 5.40, (●, ●, ●) and 0.5% (w/v) agarose gel, pH 7.40, (●, ●, ●) obtained from the UV imaging measurements ($n = 3$). The black lines represent the fits to Eq. (1).

form change of the amorphous human insulin during the dissolution study. The difference in the obtained dissolution rates of human insulin is related to the ionization state and hydrophilicity of human insulin with changing pH. Crystalline human insulin has the lowest solubility at its isoelectric point, pH 5.4 (zero net electric charge). Based on intrinsic pK_a values of the ionizable amino acids in the insulin molecule, the net charge of insulin as a function of pH has been calculated (Brange et al., 1987). At pH 3.00 the insulin molecule has a net positive charge of approximately 6, while it has a net negative charge of 3 at pH 7.40. Furthermore, UV imaging measurements have previously shown that the self-association properties of human insulin changes with changing pH, and the transport properties of human insulin in agarose hydrogels depend on the association state (Jensen et al., 2014). As apparent from the dissolution profiles (Fig. 3), there is a linear relation between the amount of dissolved insulin with time at pH 3.00 and 7.40. At pH 5.40 on the other hand the dissolution rate decline with time; it follows $\sqrt{t}$ – kinetics (Fig. 3). The dissolution rate was expected to decline with time, due to a decreasing concentration gradient. Generally, a constant concentration, corresponding to the solubility of the compound, is attained at the surface. UV imaging is cable of measuring the absorbance of the dissolved drug in the vicinity of the drug compound as a function of time. However, due to the resolution of the UV imager and the combined effect of the UV absorbance of dissolved insulin and blocking of UV light by the solid compact, it is difficult to determine the exact position of the compact surface. From the obtained UV images, the surface was estimated to be 0–56 µm from the wall of the sample holder

(the pixel-binning was 28 μm × 28 μm). The concentration of human insulin above the compact surface, at pH 3.00 and 7.40 where the apparent solubility of human insulin is relatively high, was observed to increase with time (Fig. 4A). The apparent solubility of human insulin measured in buffered solutions decreased in the following order pH 3.00 > 7.40 > 5.40 (Table 1). It was shown that a higher apparent solubility correlated in a higher dissolution rate (Table 1). The observed increase in the human insulin concentration at the surface of the compact with time indicates different dissolution kinetics at pH 3.00 and 7.40 as compared to at pH 5.40, where the human insulin concentration was near constant after approximately 60 min (Fig. 4B). Concentration–distance profiles were constructed from the obtained UV absorbance maps of human insulin dissolution at pH 3.00, 5.40, and 7.40 (Fig. 5). In comparison with the obtained apparent solubility of human insulin (Table 1), the concentration–distance profiles obtained at pH 3.00 and 7.40 show a lower concentration in the vicinity of the compact than expected. A concentration corresponding to the apparent solubility is not reached at pH 3.00 and 7.40 during the 120 min the dissolution process was followed. Contrary, a concentration corresponding to the apparent solubility of human insulin at pH 5.40 was reached after approximately 60 min. The reason why, a constant concentration was not detected at time zero, may be due to the geometry of the dissolution cell. The insulin compact has a diameter of 2 mm (id), but the width of the quartz cell containing the dissolution media (the light path) is 3 mm. Due to the geometry of the dissolution cell and the resolution of the UV imager, a delay in obtaining a constant concentration at the compact surface was observed.

3.1.1. Microenvironmental pH measurements

To have a closer look at the dissolution process, the microenvironmental pH during insulin dissolution was investigated. Suitable

Table 1
Dissolution rate (DR) of insulin in 1.5, 0.5 and 0.5% (w/v) agarose gel matrixes at pH 3.0, 5.4, and 7.4, respectively, obtained by UV imaging ($n = 3$) and the apparent solubility of insulin in buffered solutions at pH 3.00, 5.40, and 7.40 obtained at 23.0 ± 1.5 °C ($n = 3$).

	DR ± SD (μg/min/mm^2)[a]	Apparent solubility (mg/ml)[b]
Human insulin, pH 3.0	1.0 ± 0.1	>25.0
Human insulin: citric acid, pH 3.00[c]	1.6 ± 0.2	–
Human insulin, pH 5.4	$4.5 \times 10^{-3} \pm 0.2 \times 10^{-3}$	0.2
Human insulin, pH 7.4	$4.5 \times 10^{-1} \pm 0.2 \times 10^{-1}$	11.0
Bovine insulin, pH 7.4	$3.0 \times 10^{-2} \pm 0.1 \times 10^{-2}$	3.5
Protamine insulin, pH 7.4	$8.5 \times 10^{-3} \pm 0.6 \times 10^{-3}$	0.1
Protamine, pH 7.4	$5.4 \times 10^{-1} \pm 0.1 \times 10^{-1}$	>25.0

[a] DR obtained from the linear part of the dissolution profile.
[b] pH was not measured and adjusted during the experiment.
[c] Physical mixture 80:20 (w/w).

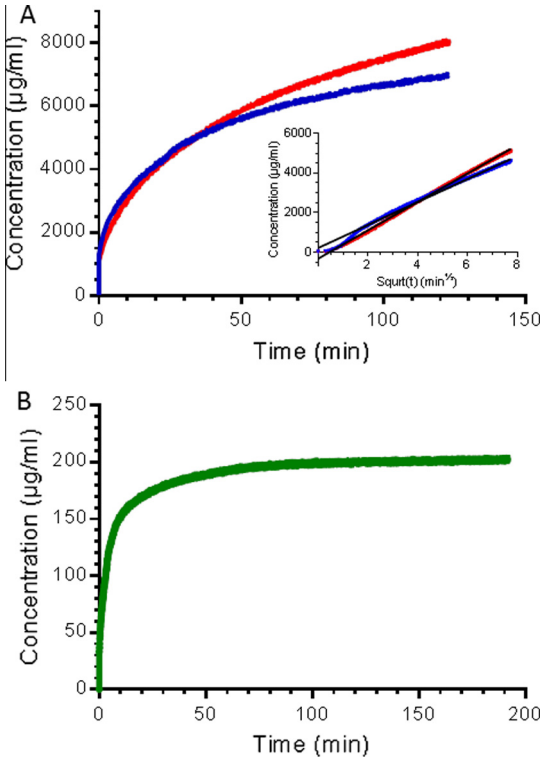

Fig. 4. Representative concentration measurements of human insulin from an area of 0.2 × 2 mm^2 above the compact surface (0–56 μm from the wall of the sample holder) during the dissolution of human insulin in (A) 1.5% (w/v) agarose gel, pH 3.00, (●) and 0.5% (w/v) agarose gel, pH 7.40, (●) and (B) 0.5% (w/v) agarose gel, pH 5.40, (●) obtained from the UV imaging measurements.

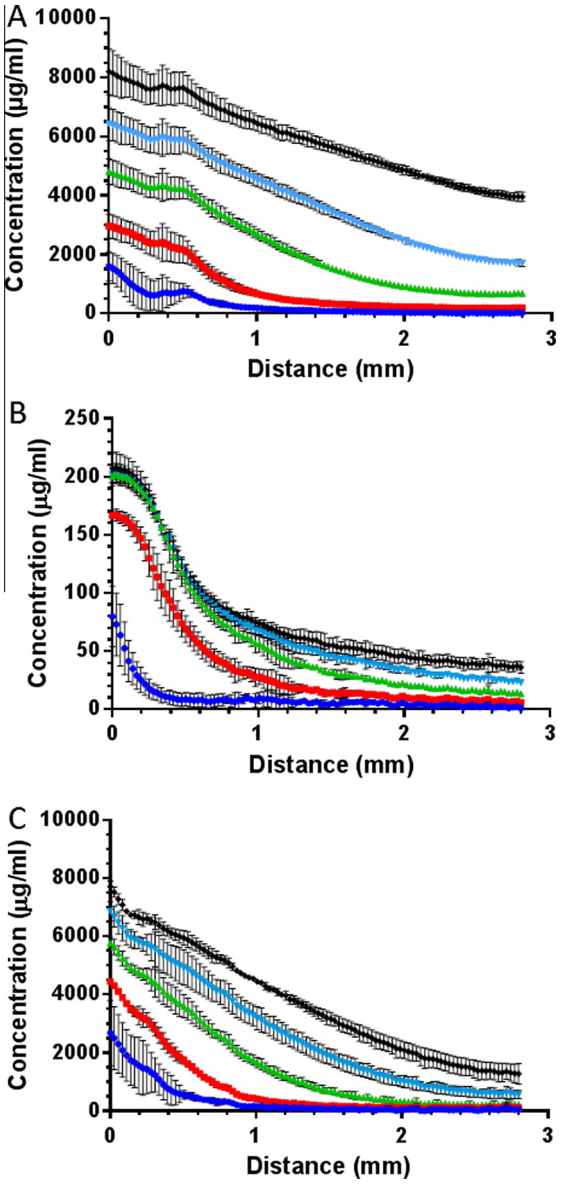

Fig. 5. Concentration–distance profiles from an area of 0.5 × 2.8 mm^2 just above the compact surface during the dissolution of human insulin in (A) 1.5% (w/v) agarose hydrogel, pH 3.00, (B) 0.5% (w/v) agarose gel, pH 5.40 and (C) 0.5% (w/v) agarose gel, pH 7.40, after 0 min (●), 10 min (■), 30 min (▲), 60 min (▼) and 120 min (♦) ($n = 3$).

pH indicators (methyl orange, methyl red, and bromothymol blue at pH 3.00, 5.40 and 7.40, respectively) were incorporated in the dissolution medium (agarose hydrogels), and the dissolution of human insulin was monitored in the visible wavelength range, where a change in pH results in a change in absorbance (and color). Insulin does not absorb light in the visible wavelength range hence changes in the absorbance during these experiments are strictly due to pH changes. Absorbance–pH profiles for methyl orange, methyl red and bromothymol blue were constructed as recently described (Østergaard et al., 2014b). The absorbance–pH profiles are shown in supplementary data Figs. A.2–A.4. A change in pH was observed in the dissolution matrix during the dissolution of human insulin at pH 3.00 and 7.40. In the dissolution experiment with an initial pH of 3.00, the local apparent pH at the surface increased from 3.07 to 3.78 during the first 30 min (Fig. 6A). At pH 5.40, the pH of the dissolution medium was near constant throughout the experiment (Fig. 7A). At pH 7.40 on the other hand, the pH had decreased to 7.05 after 60 min (Fig. 7B). The obtained results showed that the high apparent solubility and dissolution rate of human insulin at pH 3.00 and 7.40 led to a change in pH, because the buffer capacities of the dissolution media were not sufficiently high to keep the pH in the dissolution media constant. The pH in the hydrogel matrix was approaching a pH corresponding to the isoelectric point of human insulin (pI 5.4). Solid insulin is often prepared by isoelectric precipitation. In the present study, the pH in a suspension of amorphous human insulin in water (1 mg/ml) was measured to 5.5 after 5 min, it increased to 5.8 after 30 min and to 6.0 after 24 h. These pH measurements indicate that the solid human insulin used in the present study was prepared by precipitation of the human insulin from a solution at its isoelectric point. The spatial resolution of the UV imager may not be sufficient to measure the pH (and concentration) at the surface of the compact. It is suggested that the observed increase in the concentration of human insulin at the compact surface with time is due to protonation and deprotonation of the dissolved "isoelectric" insulin at pH 3.00 and 7.40, respectively, resulting in sink conditions for "isoelectric" insulin. Hence, due to this chemical conversion, a steep concentration gradient is maintained for "isoelectric" insulin at the compact surface throughout the experiment leading to the apparent zero order dissolution kinetics. The local pH at the compact surface changes with time, attaining a value in between the isoelectric point of human insulin and the initial pH of the dissolution matrix. The change in pH occurs because of the acid–base properties of human insulin and the buffering capacity of the buffered solution in the hydrogel matrix. Fig. 5 shows the concentration of human insulin (the molecular weight of human insulin: 5808 g/mol) as function of distance; it is seen that the measured human insulin concentrations were much lower than the applied buffer concentrations (0.17 and 0.067 M at pH 3.00 and 7.40, respectively). The concentrations of the acidic and basic species of the phosphate buffer (pK_a ($H_2PO_4^-$) = 6.790 (Jungas, 2006)) at e.g. pH 7.40 and 7.01 were calculated to 0.024 M $H_2PO_4^-$/0.043 M HPO_4^{2-} and 0.029 M $H_2PO_4^-$/0.038 M HPO_4^{2-}, respectively. Comparison of the measured (total) human insulin concentrations above the compact (Fig. 5) with the buffer concentrations, it is seen that the measured human insulin concentration is approximately 20

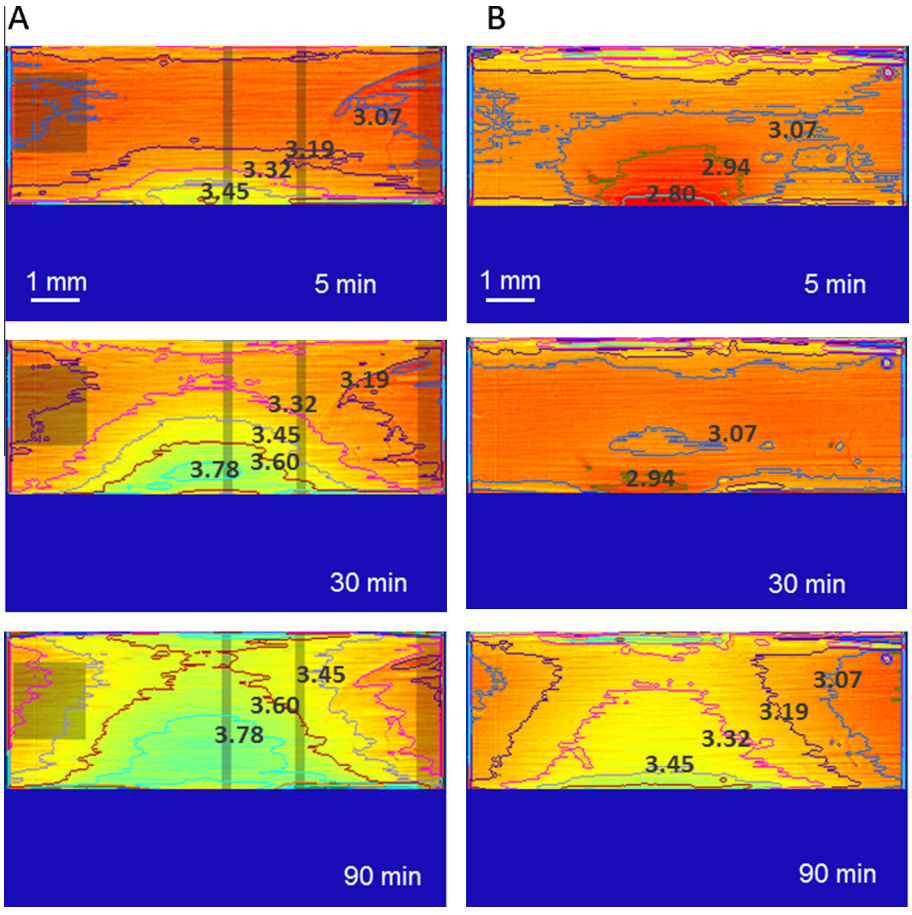

Fig. 6. Absorbance maps of (A) human insulin and (B) human insulin:citric acid (80:20) in 1.5% agarose gel, pH 3.00, containing 7.5×10^{-5} M methyl orange measured at 510 nm. The contour offset is 200 mAU and the contour interval is 50 mAU. The measurements were performed at 24.5 ± 1.5 °C. (For interpretation of the references to colour in this figure legend, the reader is referred to the web version of this article.)

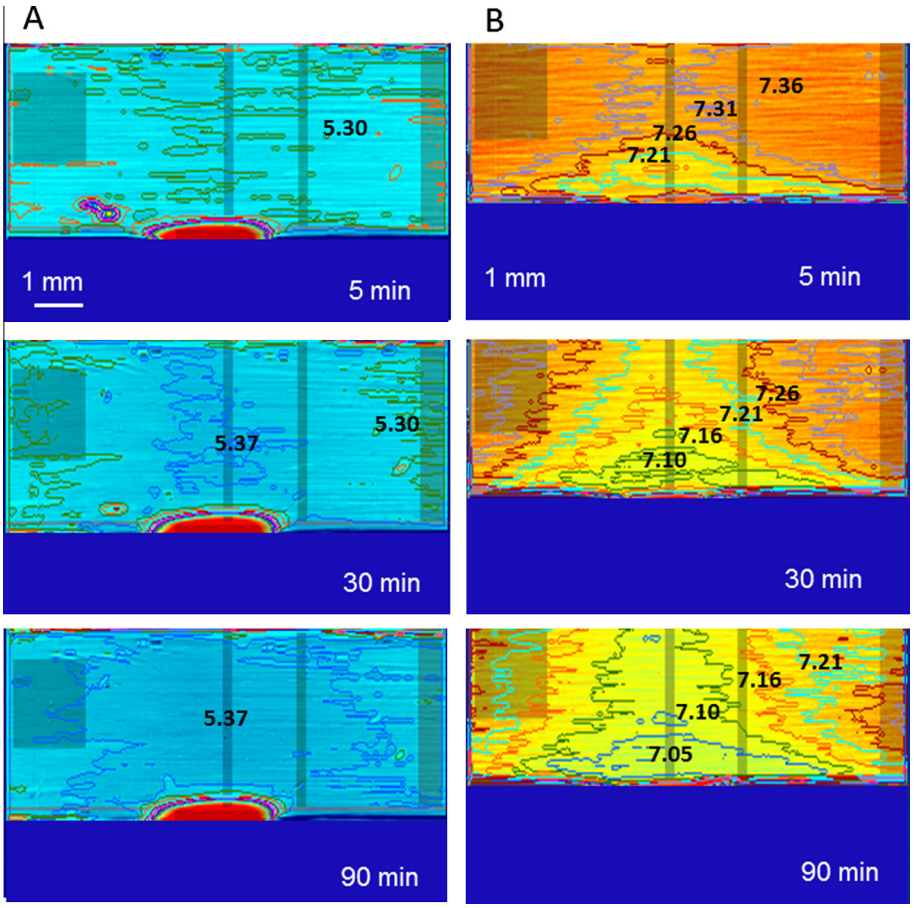

Fig. 7. Absorbance maps of human insulin dissolution in (A) 0.5% agarose gel, pH 5.4, containing 5.2×10^{-5} M methyl red (the contour offset is 150 mAU and the contour interval is 25 mAU) and (B) 0.5% agarose gel, pH 7.4, containing 6.7×10^{-5} M bromothymol blue (the contour offset is 200 mAU and the contour interval is 25 mAU). The measurements were performed at 24.5 ± 1.5 °C. (For interpretation of the references to color in this figure legend, the reader is referred to the web version of this article.)

times lower than the applied buffer concentrations after 60 min. However, taking into account the ionizable amino acids of insulin, the buffer capacity is probably not sufficient to maintain the pH constant.

To investigate further the observed pH effect at the compact surface, a pH-modifying excipient was incorporated in the compact. Citric acid (20% (w/w)) was incorporated in the human insulin compact, and the dissolution of human insulin was studied in 1.5% (w/v) agarose gel at pH 3.00. In Fig. 6B, the pH-modifying effect of citric acid in the microenvironment of the compact is shown. The pH was observed to decrease from 3.07 to 2.80 after 5 min, whereafter the pH started to increase reached a pH of 3.45 after 90 min. Presumably, due to the high solubility of citric acid, the duration of the pH modulating effect was relatively short-lived. However, citric acid was shown to alter the pH in the microenvironment of the compact resulting in an increased initial dissolution rate of human insulin (Table 1). This is also in line with the observed effect of the buffer in the dissolution experiments conducted at pH 3.00 and 7.40. In accordance with previous studies, the pH modifying effect of citric acid led to an increased release and dissolution rate of drug compounds (Hawley and Morozowich, 2010; Siepe et al., 2006). The pH modifying effect of organic acids was shown to depend both on the pK_a and the solubility of the pH modifying excipient (Bassi and Kaur, 2010). As seen for the dissolution of pure human insulin at pH 3.00 and 7.40, the dissolution profile of human insulin in the presence of citric acid was linear (supplementary data Fig. A.5.).

The ability to map local pH provides unique insight into the microenvironmental effects which directly affects insulin dissolution, release and diffusion. Microenvironmental pH effects have previously been suggested e.g. to be the reason for an observed increase in the drug release rate from PLGA-based microparticles into a 0.6% (w/w) agarose gel as compared to the release rate in agitated phosphate buffered solution (Klose et al., 2009). The developed UV–Vis imaging method may serve as a general approach for studying pH effect on drug dissolution, release and diffusion.

3.1.2. Mass transport of human insulin

To characterize the mass transport of human insulin in the hydrogel matrixes, apparent diffusion coefficients of human insulin were determined by fitting the dissolution profiles to a derivation of Fick's second law (Eq. (1)); the fit to the dissolution profiles of human insulin at pH 5.40 are shown in Fig. 3. As previously mentioned, diffusion of dissolved human insulin in the hydrogel matrixes appeared to be symmetrical around the compact surface (Fig. 2). Eq. (1) is applicable for one dimensional diffusion from a source deposited initially at a plane surface. The error made by this simplification may be reflected in the obtained apparent diffusion coefficients. In the case of constant surface concentration, which was seen in the dissolution measurement obtained at pH 5.40, the apparent diffusion coefficient of human insulin (D ± SD) was determined to $0.82 \times 10^{-10} \pm 0.09 \times 10^{-10}$ m^2/s. This value is close to the apparent diffusion coefficient of the human insulin hexamer as determined by UV imaging to $1.1 \times 10^{-10} \pm 0.1 \times 10^{-10}$ m^2/s (Jensen et al., 2014). The term apparent diffusion coefficient is applied, because insulin exists in equilibrium between different

association states (e.g. monomer, dimer, and hexamer), i.e. the diffusion coefficient may be concentration dependent.

The linear dissolution profiles obtained at pH 3.00 and 7.40 did not fit to Eq. (1). Due to the chemical conversion of dissolved "isoelectric" insulin, the mass transport of insulin in the hydrogel matrix at pH 3.00 and 7.40 may be described by the Nernst–Planck equation with a kinetic term:

$$\frac{dC}{dt} = -D \cdot \frac{d^2C}{dx^2} - u \cdot C - k \cdot C \quad (2)$$

where C is the concentration, x is the distance, u is the convection and k is the reaction rate for the protonation or deprotonation of "isoelectric" insulin. In the UV imaging *in vitro* method used in the present study there was no convective mass transport, hence the convective term in Eq. (2) may be omitted. The chemical conversion into a highly soluble insulin analog results in sink conditions and thereby a linear dissolution profile. The linear dissolution profiles may be rationalized from an expression analogous to the Noyes–Whitney equation:

$$\frac{dC}{dt} = \frac{A \cdot D}{L} \cdot (C_s - C_t) \quad (3)$$

where dC/dt is the dissolution rate, A is the surface area available for dissolution, L is the thickness of the boundary layer (in which diffusing "isoelectric" insulin is protonated/deprotonated), C_s denotes the apparent solubility of the "isoelectric" insulin at the surface of the dissolving solid, and C_t is the concentration of dissolved "isoelectric" insulin in the bulk phase at time t ($C_t = 0$). Usually, a constant diffusion layer thickness (L) is achieved by efficient stirring, high flow rates or other means of generating efficient convection. In the present system there is no convection, but instead a chemical process (protonation/deprotonation) converting the dissolving "isoelectric" insulin. The thickness of this "diffusion" layer, in the present study, is determined by the balance between the diffusion rate of "isoelectric" insulin and the rate of the chemical process (protonation/deprotonation) converting the dissolving "isoelectric" insulin. Furthermore, this chemical conversion of dissolved "isoelectric" insulin at pH 3.00 and 7.40 results in sink conditions because C_t is approaching zero. According to Eq. (3), this results in a linear dissolution profile with a slope given by $(A \cdot D/L) \cdot C_s$. The mass transport of insulin in the hydrogel at pH 3.00 and 7.40, reflected in the slope of the dissolution profile, is therefore determined by both the diffusive mass transport of human insulin in the hydrogel and the reaction rate of the protonation and deprotonation of "isoelectric" insulin in the dissolution medium near the compact surface.

Drug dissolution is highly influenced by the surrounding microenvironment. The dissolution studies performed on human insulin at pH 3.00, 5.40 and 7.40 highlights the ability of UV imaging to capture differences in dissolution behavior. The selected conditions are not all physiological relevant but serve the purpose of documenting the suitability of the UV imaging technology.

3.2. Dissolution behavior of different insulins

A variety of different insulins are available in the treatment of diabetes. In an attempt to develop an *in vitro* method that is able to differentiate between the performance of different peptide and protein drugs, the dissolution behavior of different insulins were studied. The dissolution profiles of amorphous human insulin, amorphous bovine insulin and protamine insulin into agarose hydrogel at pH 7.40 are shown in Fig. 8. Calibration curves for converting absorbance into concentration are shown in supplementary data Fig. A.1. As apparent from the dissolution profiles, amorphous human insulin has a much higher dissolution rate than

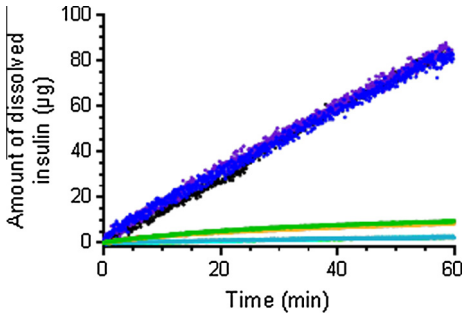

Fig. 8. Dissolution profiles for human insulin (●, ●, ●), bovine insulin (■, ■, ■) and protamine insulin (▲, ▲, ▲) in 0.5% (w/v) agarose gel pH 7.4 obtained from the UV imaging measurements ($n = 3$).

amorphous bovine insulin (Table 1). Also, the apparent solubility of human insulin was higher as compared to bovine insulin (Table 1). The initial dissolution rate depends among others on the solubility, the surface area in contact with the dissolution media, the solid state form and chemical or physical conversion of the dissolved substance. TGA measurements showed that the water content of the human insulin and bovine insulin sample was 5.9 ± 0.5 and 9.7 ± 0.3 (w/w)%, respectively ($n = 3$). The TGA measurements showed that in addition to surface water, the lyophilized bovine insulin samples also contained bound water (TA Instruments, 2014; Wang, 2000). In the lyophilized solid bovine insulin samples, surface water seemed to evaporate at temperatures ⩽75 °C while bound water was released over a temperature range up to 200 °C. In the solid human insulin samples most of the water evaporated at temperatures ⩽75 °C, and there seemed only to be surface water in these samples (supplementary data Fig. A.6). The thermogravimetric curves (supplementary data Fig. A.6) also showed that decomposition of the insulin samples began at a temperature of approximately 220 °C. In addition to the different water contents of the samples, the primary structures of human insulin and bovine insulin are dissimilar; three amino acids in the amino acid sequences of the proteins are different. Polar amino acids (threonine) in human insulin in position A8 and B30 are non-polar (alanine) in bovine insulin (Brange, 1994; Florence and Attwood, 1998; Smith, 1966). Altogether, these differences between the human insulin and bovine insulin samples may be the reason for the difference in the apparent solubility and dissolution rate observed in this study.

The dissolution behavior of the two-component system protamine insulin into agarose hydrogel at pH 7.40 was studied and compared to the dissolution behavior of human insulin and bovine insulin. Initial measurements showed that relatively high apparent solubilities and dissolution rates were obtained for the individual compounds; human insulin and protamine sulfate (Table 1). In the present study protamine insulin was prepared without adding phenol or cresol to the human insulin solution, because phenolic compounds make the UV imaging data interpretation difficult due to high UV absorbance of these compounds in the 200–300 nm range (at the same wavelengths as insulin absorbs UV light). Normally, phenol or cresol is added in the preparation of protamine insulin to obtain protamine insulin crystals (Krayenbühl and Rosenberg, 1946). Hence, the prepared protamine insulin in the present study should therefore not be mistaken with standard protamine insulin. Commercially available crystalline protamine insulin suspensions (Humulin® NPH and Insulatard®) are used in the treatment of diabetes for obtaining a sustained release of insulin for up to 24 h. A lower dissolution rate of the prepared protamine insulin sample was therefore expected. The binding mode of the protamine insulin complex is not known,

but it has been suggested that the primary function of protamine in protamine insulin formulation is to balance the overall charge of insulin (Norrman et al., 2007). Insulin and protamine co-precipitate in a 5:1 M ratio (Simkin et al., 1970). During dissolution, protamine is assumed to be released together with the hexamer approximately in a 1:1 ratio (Søeborg et al., 2009). *In vivo*, the protamine insulin crystals are packed tightly into so-called heaps which are dissolved slowly via a gel-like state (Søeborg et al., 2011).

A disadvantage of the UV imaging setup, when e.g. studying the dissolution of the two-component system protamine insulin is that it is only possible to monitor the dissolution process at a single wavelength at a time. This makes it challenging to study the dissolution rate of the drug compound of interest due to difficulties in differentiating the UV absorbance of the individual compounds. It is therefore crucial to select a suitable wavelength, where only insulin absorbs, to obtain exclusive detection of insulin. Based on UV scans of the respective compounds, it was found that protamine only absorb UV light in the 200–250 nm wavelength range (supplementary data Fig. A.7). A wavelength of 280 nm was initially selected to measure the UV absorbance of insulin, but due to a low dissolution rate, it was not possible to quantify the dissolved insulin. Instead, the dissolution measurements of protamine insulin were performed at a wavelength of 232 nm, where protamine makes only a minor contribution to the UV absorbance (less than 4%) (supplementary data Fig. A.7). Hence, the initial experiments confirmed the sustained release properties of the protamine insulin. As apparent from Fig. 8 and Table 1, the dissolution rate and apparent solubility of the insulins at pH 7.40 decreased in the following order human insulin > bovine insulin > protamine insulin. From visual inspection of the solid compacts before, during and after the dissolution experiments different solid surface behaviors of the insulins were observed. During the dissolution of protamine insulin, the solid compact was observed to swell or expand above the cup and cracks appeared in the compact surface (supplementary data Fig. A.8). XRPD measurements showed that the samples of human, bovine and protamine insulin were amorphous throughout the experiments. Hence, from the obtained results it was shown that the applied *in vitro* dissolution method was able to differentiate between the dissolution of the different insulins (human insulin, bovine insulin and protamine insulin) in the hydrogel matrixes at pH 7.40.

4. Conclusion

Real-time UV imaging was able to provide qualitative as well as quantitative information on the dissolution behavior of human insulin at different pH values and of human insulin, bovine insulin, and protamine insulin at pH 7.40. The dissolution measurements of human insulin, bovine insulin and protamine insulin in the agarose hydrogel matrixes at pH 7.40 showed that the UV imaging-based dissolution testing method was able to differentiate between the performances of the different insulins. It was shown that the dissolution rate decreased in the following order human insulin > bovine insulin > protamine insulin. Furthermore, the dissolution rate of human insulin in hydrogel matrixes was observed to be highly dependent on the pH, and the dissolution rate decreased in the following order pH 3.00 > 7.40 > 5.40. Interestingly, the amount of dissolved human insulin increased linearly with time at pH 3.00 and 7.40 indicating different dissolution kinetics than at pH 5.40. Protonation and deprotonation of dissolved "isoelectric" insulin at pH 3.00 and 7.40, respectively, maintaining a steep concentration gradient at the compact surface, was identified as the reason for the observed increase in the insulin concentration at the compact surface and the obtained linear dissolution profiles. By applying a derivation of Fick's second law, the apparent diffusion coefficient of human insulin in the hydrogel matrix at pH 5.40 was obtained. Based on the results it was seen, that the simple mathematical model (Eq. (1)) was not suitable in terms of describing the mass transport of the dissolved human insulin in the hydrogel matrix at pH 3.00 and 7.40. This confirms the importance of performing dissolution studies using a suitable *in vitro* dissolution method. Hence, the ability of the UV–Vis imaging system to measure the spatially and temporally absorbance, here reflecting the concentration and pH, in the vicinity of the compact surface provided insight into the dissolution process of insulin in hydrogel matrixes which may not have been obtained by conventional dissolution testing methods. Hence, UV–Vis imaging may provide a general method for studying pH effect on peptide and protein dissolution. By combining hydrogel matrixes with UV–Vis imaging a better understanding of the *in vivo* dissolution process of sustained release formulation intended for the subcutaneous tissue may be obtained. The current work constitutes a step toward the establishment of a compound sparing UV imaging – based dissolution testing method for peptides and proteins for subcutaneous administration.

Acknowledgements

Paraytec Ltd. (York, UK) provided access to UV imaging instrumentation. Jesper Østergaard is member of the Scientific Advisory Board of Paraytec Ltd. Economical support was obtained only from University of Copenhagen. The authors alone are responsible for the content and writing of this paper.

Appendix A. Supplementary material

Supplementary data associated with this article can be found, in the online version, at http://dx.doi.org/10.1016/j.ejps.2014.12.015.

References

Adler, J., Jayan, A., Melia, C.D., 1999. A method for quantifying differential expansion within hydrating hydrophilic matrixes by tracking embedded fluorescent microspheres. J. Pharm. Sci. 88, 371–377.
Allababidi, S., Shah, J.C., 1998. Kinetics and mechanism of release from glyceryl monostearate-based implants: evaluation of release in a gel simulating in vivo implantation. J. Pharm. Sci. 87, 738–744.
Bajwa, G.S., Hoebler, K., Sammon, C., Timmins, P., Melia, C.D., 2006. Microstructural imaging of early gel layer formation in HPMC matrices. J. Pharm. Sci. 95, 2145–2157.
Bassi, P., Kaur, G., 2010. PH modulation: a mechanism to obtain pH-independent drug release. Expert Opin. Drug Deliv. 7, 845–857.
Boetker, J.P., Savolainen, M., Koradia, V., Tian, F., Rades, T., Müllertz, A., Cornett, C., Rantanen, J., Østergaard, J., 2011. Insights into the early dissolution events of amlodipine using UV imaging and Raman spectroscopy. Mol. Pharm. 8, 1372–1380.
Brandl, F., Kastner, F., Gschwind, R.M., Blunk, T., Tessmar, J., Göpferich, A., 2010. Hydrogel-based drug delivery systems: comparison og drug diffusivity and release kinetics. J. Control. Release 142, 221–228.
Brange, J., 1994. Stability of insulin. Studies on the physical and chemical stability of insulin in pharmaceutical formulation. The Royal Danish School of Pharmacy, Copenhagen.
Brange, J., Skelbaek-Pedersen, B., Langkjær, L., Damgaard, U., Ege, H., Havelund, S., Heding, L.G., Jørgensen, K.H., Lykkeberg, J., Markussen, J., Pingel, M., Rasmussen, E., 1987. Galenics of Insulin: The Physico-chemical and Pharmaceutical Aspects of Insulin and Insulin Preparations. Springer-Verlag, New York.
Burgess, D.J., Hussain, A.S., Ingallinera, T.S., Chen, M.L., 2002. Assuring quality and performance of sustained and controlled release parenterals: AAPS workshop report, co-sponsored by FDA and USP. Pharm. Res. 19, 1761–1768.
Council of Europe, 2014. 4.1.1. Reagents, Methyl orange. European Pharmacopoeia, Council of Europe, Strasbourg.
Crank, J., 1975. The Mathematics of Diffusion. Oxford University Press, Oxford.
Florence, A.T., Attwood, D., 1998. Physicochemical principals of pharmacy. Palgrave, Hampshire.
Fyfe, C.A., Blazek-Welsh, A.I., 2000. Quantitative NMR imaging study of the mechanism of drug release from swelling hydroxypropylmethylcellulose tablets. J. Control. Release 68, 313–333.

Garcia-Ruiz, J.M., Novella, M.L., Moreno, R., Gavira, J.A., 2001. Agarose as crystallization media for proteins I: transport processes. J. Cryst. Growth 232, 165–172.
Gaunø, M.H., Vilhelmsen, T., Larsen, C.C., Boetker, J.P., Wittendorff, J., Rantanen, J., Østergaard, J., 2013. Real-time in vitro dissolution of 5-aminosalicylic acid from single ethyl cellulose coated extrudates studied by UV imaging. J. Pharm. Biomed. Anal. 83, 49–56.
Gietz, U., Arvinte, T., Mader, E., Oroszlan, P., Merkle, H.P., 1998. Sustained release of injectable zinc-recombinant hirudin suspensions: development and validation of in vitro release model. Eur. J. Pharm. Biopharm. 45, 259–264.
Hawley, M., Morozowich, W., 2010. Modifying the diffusion layer of soluble salts of poorly soluble basic drugs to improve dissolution performance. Mol. Pharm. 7, 1441–1449.
Hulse, W.L., Gray, J., Forbes, R.T., 2012. A discriminatory intrinsic dissolution study using UV area imaging analysis to gain additional insights into the dissolution behaviour of active pharmaceutical ingredients. Int. J. Pharm. 434, 133–139.
Jensen, S.S., Jensen, H., Cornett, C., Møller, E.H., Østergaard, J., 2014. Insulin diffusion and self-association characterized by real-time UV imaging and Taylor dispersion analysis. J. Pharm. Biomed. Anal. 92, 203–210.
Jungas, R.L., 2006. Best literature values for the pK of carbonic and phosphoric acid under physiological conditions. Anal. Biochem. 349, 1–15.
Kadima, W., Øgendal, L., Bauer, R., Kaarsholm, N., Brodersen, K., Hansen, J.F., Porting, P., 1993. The influence of ionic strength and pH on the aggregation properties of zinc-free insulin studied by static and dynamic laser light scattering. Biopolymers 33, 1643–1657.
Kazarian, S.G., Ewing, A.V., 2013. Applications of Fourier transform infrared spectroscopic imaging to tablet dissolution and drug release. Expert Opin. Drug Deliv. 10, 1207–1221.
Kazarian, S.G., van der Weerd, J., 2008. Simultaneous FTIR spectroscopic imaging and visible photography to monitor tablet dissolution and drug release. Pharm. Res. 25, 853–860.
Kimber, J.A., Kazarian, S.G., Stepanek, F., 2011. Microstructure-based mathematical modelling and spectroscopic imaging of tablet dissolution. Comput. Chem. Eng. 35, 1328–1339.
Kinnunen, H.M., Mrsny, R.J., 2014. Improving the outcomes of biopharmaceutical delivery via the subcutaneous route by understanding the chemical, physical and physiological properties of the subcutaneous injection site. J. Control. Release 182, 22–32.
Klose, D., Azaroual, N., Siepmann, F., Vermeersch, G., Siepmann, J., 2009. Towards more realistic in vitro release measurement techniques for biodegradable microparticles. Pharm. Res. 26, 691–699.
Krayenbühl, C.H., Rosenberg, T.H., 1946. Crystalline protamine insulin. Rep. Steno Mem. Hosp. Nord. Insulin Lab. 1, 60–73.
Lee, S.J., Pishko, G.L., Astary, G.W., Mareci, T.H., Sarntinoranont, M., 2009. Characterization of an anisotropic hydrogel tissue substrate for infusion testing. J. Appl. Polym. Sci. Symp. 114, 1992–2002.
Levick, J.R., 1987. Flow through interstitium and other fibrous matrices. Quart. J. Exp. Physiol. 72, 409–437.
Liang, S., Xu, J., Weng, L., Dai, H., Zhang, X., Zhang, L., 2006. Protein diffusion in agarose hydrogel in situ measured by improved refractive index method. J. Control. Release 115, 189–196.
Lin, J.H., 2009. Pharmacokinetics of biotech drugs: peptides, proteins and monoclonal antibodies. Curr. Drug Metab. 10, 661–691.
Lorber, B., Sauter, C., Theobald-Dietrich, A., Moreno, A., Schellenberger, P., Robert, M.C., Capelle, B., Sanglier, S., Potier, N., Giege, R., 2009. Crystal growth of proteins, nucleic acids, and viruses in gels. Prog. Biophys. Mol. Biol. 101, 13–25.
Maaloum, M., Pernodet, N., Tinland, B., 1998. Agarose gel structure using atomic force microscopy: Gel concentration and ionic strength effects. Electrophoresis 19, 1606–1610.
Martinez, M., Rathbone, M., Burgess, D., Huynh, M., 2008. In vitro and in vivo considerations associated with parenteral sustained release products: a review based upon information presented and points expressed at the 2007 controlled release society annual meeting. J. Control. Release 129, 79–87.
McDonald, T.A., Zepeda, M.L., Tomlinson, M.J., Bee, W.H., Ivens, I.A., 2010. Subcutaneous administration of biotherapeutics: current experience in animal models. Curr. Opin. Mol. Ther. 12, 461–470.
Niederquell, A., Kuentz, M., 2014. Biorelevant dissolution of poorly soluble weak acids studied by UV imaging reveals ranges of fractal-like kinetics. Int. J. Pharm. 463, 38–49.
Nielsen, L.H., Gordon, S., Pajander, J.P., Østergaard, J., Rades, T., Müllertz, A., 2013. Biorelevant characterisation of amorphous furosemide salt exhibits conversion to a furosemide hydrate during dissolution. Int. J. Pharm. 457, 14–24.
Norrman, M., Hubalek, F., Schluckebier, G., 2007. Structural characterization of insulin NPH formulations. Eur. J. Pharm. Sci. 30, 414–423.
Nott, K.P., 2010. Magnetic resonance imaging of tablet dissolution. Eur. J. Pharm. Biopharm. 74, 78–83.
Østergaard, J., Meng-Lund, E., Larsen, S.W., Larsen, C., Petersson, K., Lenke, J., Jensen, H., 2010. Real-time UV imaging of nicotine release from transdermal patch. Pharm. Res. 27, 2614–2623.
Østergaard, J., Ye, F., Rantanen, J., Yaghmur, A., Larsen, S.W., Larsen, C., Jensen, H., 2011. Monitoring lidocaine single-crystal dissolution by ultraviolet imaging. J. Pharm. Sci. 100, 3405–3410.
Østergaard, J., Wu, J.X., Naelapaa, K., Boetker, J.P., Jensen, H., Rantanen, J., 2014a. Simultaneous UV imaging and Raman spectroscopy for the measurement of solvent-mediated phase transformations during dissolution testing. J. Pharm. Sci. 103, 1149–1156.
Østergaard, J., Jensen, H., Larsen, S.W., Larsen, C., Lenke, J., 2014b. Microenvironmental pH measurement during sodium naproxenate dissolution in acidic medium by UV/vis imaging. J. Pharm. Biomed. Anal. 100, 290–293.
Pluen, A., Netti, P.A., Jain, R.K., Berk, D.A., 1999. Diffusion of macromolecules in agarose gels: comparison of linear and globular configurations. Biophys. J. 77, 542–552.
Qiao, N., Wang, K., Schlindwein, W., Davies, A., Li, M., 2013. In situ monitoring of carbamazepine–nicotinamide cocrystal intrinsic dissolution behaviour. Eur. J. Pharm. Biopharm. 83, 415–426.
Richardson, J.C., Bowtell, R.W., Mäder, K., Melia, C.D., 2005. Pharmaceutical applications of magnetic resonance imaging (MRI). Adv. Drug Deliv. Rev. 57, 1191–1209.
Richter, W.F., Bhansali, S.G., Morris, M.E., 2012. Mechanistic determinants of biotherapeutics absorption following SC administration. AAPS J. 14, 559–570.
Sarnes, A., Østergaard, J., Jensen, S.S., Aaltonen, J., Rantanen, J., Hirvonen, J., Peltonen, L., 2013. Dissolution study of nanocrystal powders of a poorly soluble drug by UV imaging and channel flow methods. Eur. J. Pharm. Sci. 50, 511–519.
Siepe, S., Lueckel, B., Kramer, A., Ries, A., Gurny, R., 2006. Strategies for the design of hydrophilic matrix tablets with controlled microenvironmental pH. Int. J. Pharm. 316, 14–20.
Simkin, R.D., Cole, S.A., Ozawa, H., Magdoff-Fairchild, B., Eggena, P., Rudko, A., Low, B.W., 1970. Precipitation and crystallization of insulin in the presence of lysozyme and salmine. Biochim. Biophys. Acta 200, 385–394.
Smith, L.F., 1966. Species variation in the amino acid sequence of insulin. Am. J. Med. 40, 662–666.
Søeborg, T., Rasmussen, C.H., Mosekilde, E., Colding-Jørgensen, M., 2009. Absorption kinetics of insulin after subcutaneous administration. Eur. J. Pharm. Sci. 36, 78–90.
Søeborg, T., Rasmussen, C.H., Mosekilde, E., Colding-Jørgensen, M., 2011. Bioavailability and variability of biphasic insulin mixtures. Eur. J. Pharm. Sci.
Swabb, E.A., Wei, J., Gullino, P.M., 1974. Diffusion and convection in normal and neoplastic tissues. Cancer Res. 34, 2814–2822.
Swartz, M.A., Fleury, M.E., 2007. Interstitial flow and its effects in soft tissues. Annu. Rev. Biomed. Eng. 9, 229–256.
TA Instruments, 2014. Thermal solutions. Separation of free and bound water in pharmaceuticals. <http://www.tainstruments.co.jp./application/pdf/Thermal_Library/Thermal_Solutions/TS017.PDF> (accessed on 05.03.14).
Tinland, B., Pernodet, N., Weill, G., 1996. Field and pore size dependence of the electrophoretic mobility of DNA: a combination of fluorescence recovery after photobleaching and electric birefringence measurements. Electrophoresis 17, 1046–1051.
Wang, W., 2000. Lyophilization and development of solid protein pharmaceuticals. Int. J. Pharm. 203, 1–60.
Xiong, J.Y., Narayanan, J., Liu, X.Y., Chong, T.K., Chen, S.B., Chung, T.S., 2005. Topology evolution and gelation mechanism of agarose gel. J. Phys. Chem. B 109, 5638–5643.
Ye, F., Yaghmur, A., Jensen, H., Larsen, S.W., Larsen, C., Østergaard, J., 2011. Real-time UV imaging of drug diffusion and release from Pluronic F127 hydrogels. Eur. J. Pharm. Sci. 43, 236–243.
Ye, F., Larsen, S.W., Yaghmur, A., Jensen, H., Larsen, C., Østergaard, J., 2012a. Drug release into hydrogel-based subcutaneous surrogates studied by UV imaging. J. Pharm. Biomed. Anal. 71, 27–34.
Ye, F., Larsen, S.W., Yaghmur, A., Jensen, H., Larsen, C., Østergaard, J., 2012b. Real-time UV imaging of piroxicam diffusion and distribution from oil solutions into gels mimicking the subcutaneous matrix. Eur. J. Pharm. Sci. 46, 72–78.